Solution Properties of Glycogen. 2. Semidilute Solutions†

Catalina E. Ioan,‡ Thomas Aberle, and Walther Burchard*

Institute of Macromolecular Chemistry, University of Freiburg, 79104 Freiburg, Germany

Received July 8, 1999; Revised Manuscript Received September 16, 1999

ABSTRACT: Interparticle interaction and structure of glycogen from a shell fish (mussels) were studied in water and 0.5 N NaOH by static and dynamic light scattering and viscometry. A concentration regime up to 30% w/v was covered. Beyond the overlap concentration a large-scale clustering was observed which was interpreted as associates. Glycogen is a natural representative for hyperbranched polysaccharides. Interpretation of data was made for the inverse forward scattering (at scattering angle $\theta = 0$). The measured quantities could be separated into interparticle interaction contributions and a change in the particle structure when the concentration was increased. A master curve was obtained for $X < 1$ when plotting $M_w/M_{app}(c)$ against $X = A_2M_wc = c/c^*$, where $M_{app}(c)$ is the apparent (measured) molar mass at concentration c. This master curve agrees within experimental error with that for amylopectin. Deviations to a flatter curve were found when $X > 1$. Simultaneously to the forward scattering the apparent radius of gyration $R_{app}(c)$ was measured. The influence of interparticle interaction could be split off, and the true $R_g(c)$ was obtained. Up to $X = 1$ no change was observed, but at $X > 1$ a sharp increase in the dimensions by 2−3 orders in magnitude was found. Similar behavior was found also in dynamic light scattering where a slow mode of motion became noticeable at $X > 2$. These three effects—deviation from the interaction master curve, increase in $R_g(c)$, and development of a slow mode of motion—give strong evidence for onsetting association. The specific viscosity showed common behavior with a weak increase in the dilute regime and a strong increase in the semidilute regime. The kink points were found with $c[\eta] = 0.57$ and 0.82 for NaOH and H_2O, respectively, much smaller than $c[\eta] \cong 4$ as observed for most linear macromolecules. However, a very good agreement with latex particles was found.

Introduction

In the past the characterization of polymers was focused mainly on the properties in *dilute* solution. In that concentration range the individual macromolecules are well isolated from each other. Thus, the structure of single molecules can be studied and allows us to determine the macromolecular architecture. More interesting in application, however, is the higher concentrated domain. In this regime the interparticle interaction gains dominating influence on the properties of the systems. As a result, the measured molecular parameters are strongly affected by these interactions. The question arises whether the influence of interaction can be separated off, which would lead to the properties of the macromolecules or aggregated particles at a given concentration. Because of the work of de Gennes,[1] the problems of semidilute solutions of *linear chains* can be considered as widely solved. Little is known, however, of branched structures.[2,3] As was shown in previous papers,[4,5] special effects are to be expected since the branching points represent obstacles and prevent a full interpenetration of segments from different particles, which is an essential presumption in de Gennes scaling theory. Nonetheless, as for linear chains, the overlap concentration plays a dominant role also for the branched materials. To determine this key parameter, it remains imperative to study first the dilute solution properties. This was done for glycogen in part 1.

Glycogen is a branched α(1,4), α(1,6) glucan that can be considered as a hyperbranched macromolecule of the $A(^{B_1}_{B_2})$ type polycondensate.[6] In the present contribution the investigation is extended to the regime of semidilute and concentrated solutions up to 30% (mass/volume). The overlap concentration can be defined in different ways, as was outlined previously.[2] The following treatment of data is based mainly on static properties. Here it is appropriate to use the definition[7]

$$c^* \equiv [A_2M_wc]^{-1} \tag{1}$$

The data of A_2 and M_w are known from the study in dilute solution (paper 1).[8] In a study of dynamic properties, on the other hand, the choice of $c_\eta^* \equiv 1/[\eta]$ is often more successful. The two overlap concentrations often deviate from each other, in particular for branched macromolecules.[9]

The already mentioned deviations in behavior of branched polymers from semidilute linear chains can be expected to be particularly large for macromolecules of a high segment density. We have chosen glycogen, with a branching density of about 8% (i.e., 8% branching points in the polymer). The results are of special interest when compared with the results from amylopectin.[4] Like in glycogen the monomer unit in amylopectin is the anhydroglucose, and they are connected in the same way as in glycogen, but with the lower branching density of 4−4.5%.

Theory

The applied experimental techniques were static and dynamic light scattering (LS). For large particles the scattering intensities in static LS and the time correlation functions (TCF) in dynamic LS are strongly angular dependent. This angular dependence gives in static light scattering information on the shape and the internal structure of the samples and in dynamic light scattering

† Dedicated to Dr. Karel Dušek, Instiute of Macromolecular Chemistry, Czech Academy of Science, on the occasion of his 70th birthday.

‡ Permanent address: "P. Poni" Institute of Macromolecular Chemistry, 6600 Iasi, Romania.

10.1021/ma991112h CCC: $18.00
Published on Web 11/13/1999

the translational and internal mobility. Two differently averaged molecular radii are determined: In static LS the radius of gyration R_g is measured from the initial part of the angular dependence. In dynamic LS a hydrodynamic radius R_h is obtained from the translational diffusion coefficient D according to the Stokes−Einstein relationship

$$R_h = \frac{kT}{6\pi\eta_0 D} \tag{2}$$

The diffusion coefficient is obtained from the initial decay of the field TCF, $g_1(t)$,[10] which is approximatly given as

$$g_1(t) \cong \exp(-q^2 Dt)$$

where $q = (4\pi n_0/\lambda_0)\sin(\theta/2)$ is the scattering vector that is related to the scattering angle θ and the wavelength λ_0 of the light used; n_0 is the refractive index of the solvent.

The two radii are clearly defined only at zero concentration ($c \rightarrow 0$), but the mentioned two slopes can be measured also at finite concentration. The observed concentration dependence is controlled by interparticle interactions. In the present study good solvent conditions are valid, where the interactions are repulsive.

The repulsion among the particles increases with the concentration. The interaction can be measured without any assumptions from the so-called forward scattering of static LS. To this end the scattering intensity R_θ has to be extrapolated to zero scattering angle. Statistical thermodynamics show[11,12]

$$R_{\theta=0} = KcRT\left(\frac{\partial c}{\partial \pi}\right) \tag{3}$$

where $RT(\partial c/\partial\pi)$ is the osmotic compressibility. When the osmotic pressure π is developed in a virial series, one obtains eq 4

$$\left(\frac{Kc}{R_{\theta=0}}\right)_c \equiv \frac{1}{M_{app}(c)} = \left(\frac{1}{RT}\right)\left(\frac{\partial \pi}{\partial c}\right) = \frac{1}{M_w}[1 + 2X + 3g_a X^2 + 4h_a X^3] \tag{4}$$

with

$$X = A_2 M_w c \equiv c/c^* \tag{5}$$

$c^* = (A_2 M_w)^{-1}$ is the overlap concentration, and K is the common contrast factor in static LS. The forward scattering multiplied by the second virial coefficient A_2[3,9] gives

$$A_2 \frac{R_{\theta=0}}{K} = A_2 RT\left(\frac{\partial c}{\partial \pi}\right) = \frac{X}{1 + 2X + 3g_a X^2 + 4h_a X^3} \tag{6}$$

In this relationship the scaling assumption has been used that all higher virial coefficients can be expressed in terms of the second one. This behavior was shown to hold hard spheres, flexible linear chains, and other various particle architectures.[3,9,13] At high concentrations more than only three virial coefficients have to be taken into account, but the virial representation works exactly only for hard spheres but eventually fails for other structures. Positive and negative coefficients of increasing value occur and finally diverge.[11,14] The present parameters g_a and h_a are to be considered solely as empirical fitting parameters.[9] The left side and the parameter X can be measured without introducing assumptions.

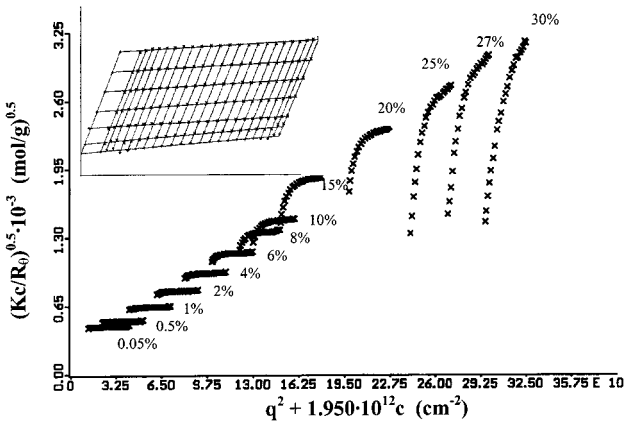

Figure 1. Berry plot of static light scattering intensities from mussels glycogen in a concentration range of 0.05% ≤ c ≤ 30% (w/v). Inset: dilute behavior ($c \leq 0.1\%$): $M_w = 7.01 \times 10^6$ g/mol; $R_g = 25$ nm, $A_2 = 2.81 \times 10^{-6}$ mol mL/g^2, solvent 0.5 N NaOH. The figures at the curves indicate the concentration applied.

Experimental Section

Sample. Glycogen from mussel (type VII) was a product of Sigma. Its dry substance content was determined in a moisture analyzer (MA 40, Sartorius, Germany). The obtained value was 86%.

Static light scattering (SLS) measurements were made with a computerized and modified SOFICA photogoniometer (G. Baur, Instrumentenbau, Hausen, Germany). The goniometer was equipped with a 2 mW He−Ne laser (632.8 nm). Measurements were made in an angular range from 30° to 145°, in steps of 5°, at 20 °C. As a solvent 0.5 N NaOH was used. The refractive index increment was measured in a Brice Phoenix refractometer and gave dn/dc = 0.142 mL/g. In a few cases also water (Millipore quality, 18.2 mΩ) was used with an dn/dc = 0.151 mL/g.

Dynamic light scattering (DLS) measurements were made with an ALV photogoniometer (ALV, Langen, Germany) and an ALV 5000 correlator (in the angular range from 30° to 150° in steps of 10°).

All solutions were filtered through Millipore filters (1.2 μm) before measurement.

Viscosity measurements were made with an automatic Ubbelohde viscometer (Schott, Germany) at 20 °C in 0.5 N NaOH and in water. A capillary of 0.63 mm in diameter was used. Shear gradient independence was checked with a CS Bohlin rheometer.

Results

Static Behavior. Molecular Parameters. Figure 1 shows a Berry diagram from glycogen in 0.5 M NaOH in the whole concentration range of 0.05% ≤ c ≤ 30%. From this Berry plot the molar mass, radius of gyration, and the second virial coefficient were determined as usual from the dilute regime (see inset of Figure 1), which gave $M_w = 7.01 \times 10^6$ g/mol, $R_g = 25$ nm, and $A_2 = 2.81 \times 10^{-6}$ mol mL/g^2. With these data an overlap concentration of $c^* = (A_2 M_w)^{-1} = 50.8$ mg/mL (≅5% w/v) is obtained. This value is used in the following as scaling factor for the reduced concentration $X \equiv c/c^*$.

Up to a concentration of about 8% (w/v) the Berry plot shows common behavior; only at the smallest angle for the 8% solution a slight downturn was obtained. This downturn became increasingly more pronounced when the concentration was increased, and finally curves were

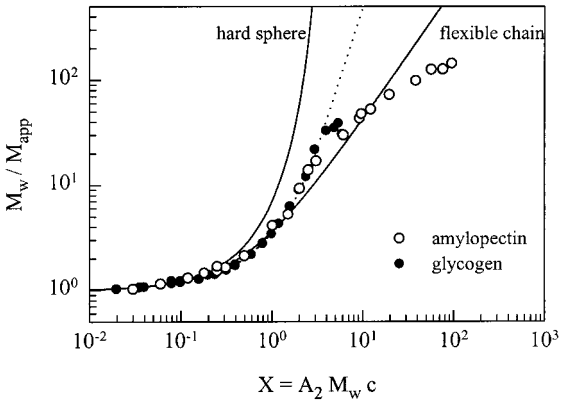

Figure 2. Plot of $M_w/M_{app}(c)$ against the scaled concentration $X \equiv c/c^* \equiv A_2M_wc$. $M_{app}(c)$ is the apparent molar mass at concentration c. Its value is determined by the osmotic compressibility as $M_{app} = RT(\partial c/\partial \pi)$ and is given by eq 4′. The full lines represent the theoretical curves for hard spheres[15] and flexible linear chains.[16] The symbols refer to experimental data. The dashed line represents a curve obtained with starches of various degrees of polymerization and to glycogen, before the onset of a turnover. This turnover occurs at larger X for high DP hyperbranched macromolecules than for smaller ones. The dashed line thus represents a master curve that is obeyed by different sizes of the branched macromolecule.

obtained that appear to be composed of two components. The steep slope at low angles indicates the presence of large particles which are to be considered as associates of several glycogen macromolecules, while the flat slope at large scattering angles may be assigned to the apparent radius of gyration of the individual molecules.

Reduced Osmotic Modulus. The values in the Berry plot for the various concentration at zero scattering angle ($q = 0$, forward scattering) may be denoted as $[1/M_{app}(c)]^{1/2}$. Then with eqs 1, 4, and 5 one finds

$$\frac{M_w}{M_{app}(c)} = \left(\frac{M_w}{RT}\right)\left(\frac{\partial \pi}{\partial c}\right) = [1 + 2X + 3g_aX^2 + 4h_aX^3] \quad (4')$$

Multiplying eq 4′ by the molar mass M_w (determined from the limit at zero concentration), one obtains a dimensionless quantity $M_w/M_{app}(c)$ that will be called the *reduced osmotic modulus*. It describes the osmotic pressure that is needed to bring the particles closer together when the concentration is increased. For hard spheres the increase of the interaction diverges when the spheres start to touch each other. This happens when $X > 3$.[15] (Note: for hard spheres one has $X = 4\phi$, where ϕ is the volume fraction of the spheres. Close sphere packing is reached at approximately $\phi \cong 0.63$.) Such divergence does not occur with coils from linear flexible chains, because the coils can interpenetrate.[7,16] Although the repulsion among the segments still remains, the overall repulsion will be much weaker in these cases than for hard spheres. A situation between these two limits should be found when a full interpenetration of coils is prevented by obstacles, as for instance by branching points. This effect has been indeed observed (Figure 2).[3,4b,9] When plotting the reduced osmotic modulus $M_w/M_{app}(c)$ in a double-logarithmic scale against the reduced concentration X,[4b,13] we found for each of the various molecular topologies universal curves, i.e., master curves in which the same curve is obtained when the concentration for a given molar mass or the molar mass and the concentration were varied, and even when the solvent is changed, provided the limit of good solvent behavior, i.e., $A_2 > 0$ is preserved.[5] However, beyond a certain value of $X > 1$ the curve for glycogen and amylopectin becomes flatter, and in other cases the curves pass through a maximum and then decay drastically toward zero.

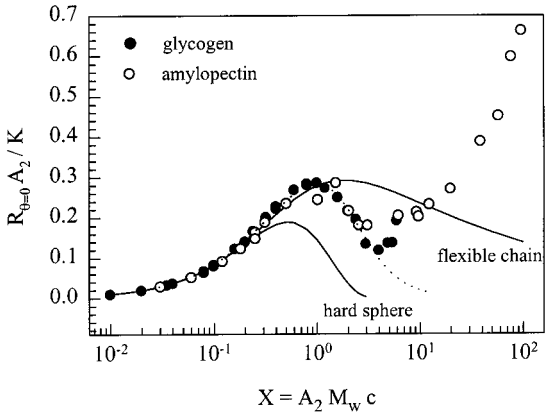

Figure 3. Normalized forward scattering (at $\theta = 0$) as a function of the scaled concentration $X = c/c^*$ (see eq 4). The full lines correspond to theories for hard spheres and flexible chains. The dotted line represents the master curve for amylopectin and glycogen; the strong increase at large X corresponds to the flat curve section in Figure 2 and indicates association. $M_{w,Ap} = 70 \times 10^6$ g/mol, $M_{w,glycogen} = 7.01 \times 10^6$ g/mol.

Forward Scattering. The differences in behavior of the various architectures are much better seen when the normalized forward scattering of eq 4 is used and plotted against X.[9,13b] This is shown in Figure 3 for the glycogen of this study and is compared with the data obtained for amylopectin.[4a] The theoretical curves for hard spheres[15] and linear flexible chains[16] are shown again as references. The effect of the high segment density for glycogen is clearly seen. As expected, the glycogen curve is positioned closer to the hard sphere than the amylopectin curve. The two curves for amylopectin and glycogen are well described in the $X \leq 3$ regime by eq 4 with the sets of $g_a = 0.18$, $h_a = 0.03$ and $g_a = 0.001$, $h_a = 0.127$ for glycogen and amylopectin, respectively. These coefficients have to be considered solely as best fitting parameters, and the description of the cures is not particularly sensitive to the value of g_a. The two coefficients turned out being strongly correlated to each other, and the actual fit is not very sensitive to changes in the value of g_a. Therefore, it is not justified to conclude poor solution behavior in the case of amylopectin. The actual values for A_2 were positive and showed good solution properties (see part 1).[8] The curves pass through a maximum at $X \cong 1$ and according to eq 4 should then decay continuously with increasing X as indicated by the dotted line. However, at $X > 3$ an upturn occurs again. This upturn corresponds to the flatter region shown in Figure 2. These deviations can be attributed to association as will be shown in the discussion.

Dynamic Light Scattering. In dynamic light scattering a time correlation function (TCF) is measured, which decays exponentially with the decay time. From the initial decay constant a translational diffusion coefficient $D_{app}(q)$ is obtained, which for large particles can also depend on the scattering angle θ (via $q = (4\pi n_0/\lambda_0) \sin \theta/2$). This diffusion coefficient has to be considered as an apparent one, which contains also contributions from internal segment motions.[10,17] Figure 4 shows as an example such an angular dependence for

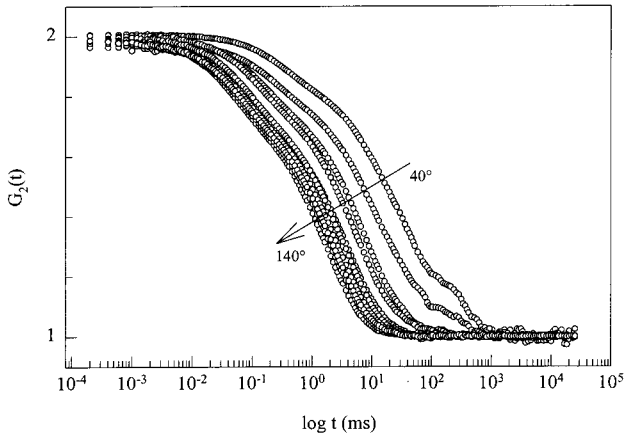

Figure 4. Angular dependence of time correlation functions in dynamic light scattering from a 20% glycogen solution. A fast and a slow mode of motion are clearly recognized.

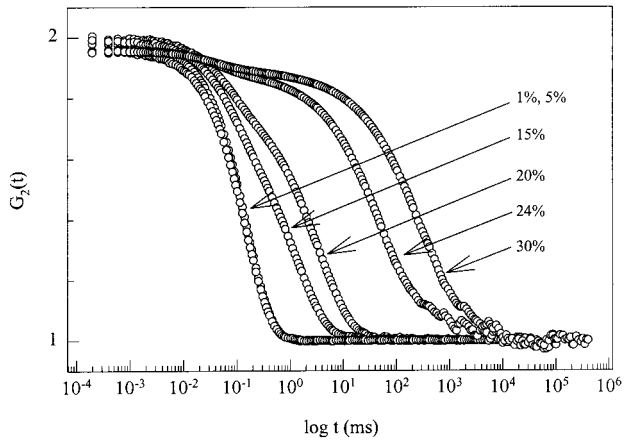

Figure 5. Concentration dependence of time correlation functions at 90° of glycogen solutions.

a 20% glycogen solution. The true mutual diffusion coefficient $D(0,c)$ is obtained at zero angle. The mutual diffusion coefficient depends in general on the concentration and becomes the *z*-average translational diffusion coefficient D_z at $c = 0$. Mostly a linear relationship represents a good approximation that makes possible a reliable extrapolation to zero concentration.

$$D(0,c) = D_z(1 + kc) \tag{7}$$

Figure 5 shows correlation curves at different concentrations for the scattering angle of 90°. Up to the overlap concentration c^* (5%) the expected single-exponential decay is observed. At higher concentrations a second mode appears, which with increasing concentration moves toward longer delay times. The slow motion gives indications to associates that grow with increasing concentration, while the fast motion corresponds to the diffusion of nonassociated molecules. The quantitative analysis of the TCF curves by fits with William−Watts[18] (stretched exponential) function indicated two slow modes, which, however, will be combined in our discussion as only one slow mode. Figure 6 shows in a normalized plot the concentration dependence of these components. The fast motion slightly increases with *c*, while the two slow motions are enormously slowed by 5 decades.

Viscosity. The viscosities were measured by capillary viscometry as described in the experimental part. The result of the specific viscosity η_{sp} against $c[\eta]$ is shown

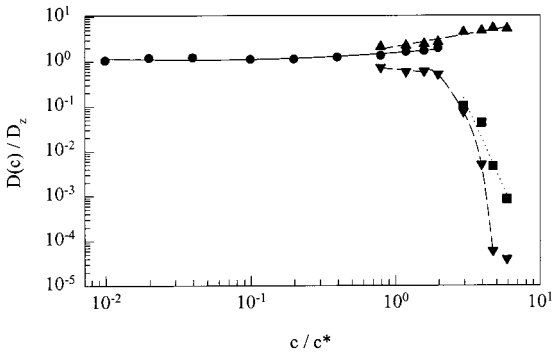

Figure 6. Normalized mutual diffusion coefficient $D(c)$ as a function of $c/c^* \equiv X$. The different curves correspond to the fast and slow modes of translational motion. The data result from a Williams−Watts analysis of the time correlation functions. The best fit was made with three modes (one fast mode and two slow modes). The split in the two slow modes may be artifact of fitting. The averages of the two slow modes were considered in the discussion. The filled circles refer to the cumulant fit. Triangle up, fast mode; triangle down and square, slow modes.

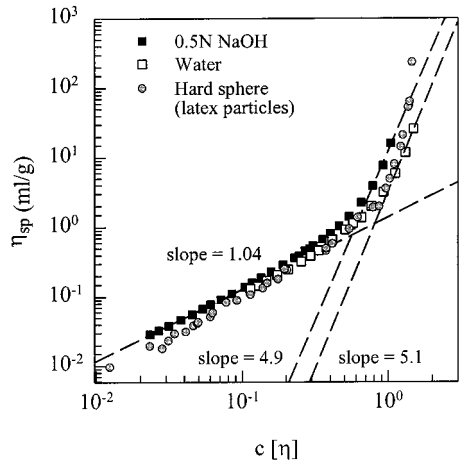

Figure 7. Dependence of the specific viscosity $(\eta - \eta_s)/\eta_s$ of glycogen as a function of $c[\eta]$, where $[\eta]$ is the intrinsic viscosity. Glycogen intersection point: 0.5 N NaOH: $[\eta] = 6.9$ mL/g; $c[\eta] = 0.57$ ($c_\eta^* = 0.082$ g/mL); $\eta_{sp} = 0.77$ mL/g. Water: $[\eta] = 6.6$ mL/g; $c[\eta] = 0.82$ ($c_\eta^* = 0.122$ g/mL); $\eta_{sp} = 1.16$ mL/g.

in Figure 7. The points of measurements can be fitted by two asymptotic lines with exponents of $m = 1.04$ and $m = 4.82$. The one represents common dilute solution behavior, whereas the steep increase is an indication for entanglement.[19] The two lines intersect at $c[\eta] = 0.57$, which corresponds to a concentration of $c = 82$ g/L and $\eta_{sp} = 0.773$ mL/g. This intersection point can be considered as the concentration, when partial interpenetration becomes hydrodynamically effective. At this point it is worth mentioning that this concentration is about 60% larger than c^*, i.e., $c_{intersect} = 1.64c^*$. Figure 7 contains also the results from measurements in water and for comparison data from latex particles in water. The curve in water agrees with that in NaOH at low concentrations, but strong hydrodynamic interaction due to the hairy region in the outer shells of the particle becomes effective somewhat later.

Discussion

The findings with concentrated glycogen and amylopectin solutions display unexpected deviations in the interparticle interaction (osmotic modulus), in dynamic

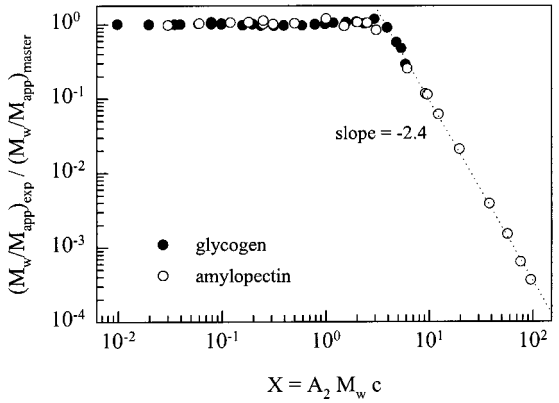

Figure 8. Ratio of the measured osmotic modulus to that of the master curve (dashed line in Figure 2) for glycogen (filled circles) and amylopectin (open circles) as a function of the scaled concentration $X = c/c^*$.

light scattering, and in viscosity behavior, for which so far no theory has been developed. In the following we discuss several aspects of interpretation, which eventually led us to a rather definite conclusion. We start with the osmotic modulus, consider then the radius of gyration and the hydrodynamic radius as a function of c and finally combine these three quantities. As a last point the viscosity behavior is discussed.

Reduced Osmotic Modulus. The flattening of the curve in Figure 2 occurs when the overlap concentration is exceeded. Following the conception of de Gennes[1] for flexible linear chains, the domains of macromolecules overlap due to the chain interpenetration. A transient gel is obtained, in which the points of entanglements are not fixed like it is the case for the cross-links in permanent gels. A correlation length $\xi(c)$ is found that decreases with increasing concentration. As a consequence, the excluded volume effect becomes gradually screened out until θ-conditions ($A_2 = 0$) are obtained. Thus, the deviation from the master curve (dashed line) in Figure 2 could be caused by excluded volume screening also for the branched polysaccharide.[2,4b] To get a deeper insight, we divided the measured osmotic modulus curve by that of the master curve. The dashed line in Figure 2 was obtained with amylopectin samples of different molar mass in two solvents and is within experimental error the same also for glycogen. We thus consider this curve as a master curve. The result is shown in Figure 8 for glycogen and amylopectin. The corresponding mathematic relationship is given as

$$\frac{[M_w/M_{app}(c)]_{exp}}{[M_w/M_{app}(c)]_{master}} = \frac{[1 + 2A_2M_wc + 3A_3M_wc^2 + 4A_4M_wc^3]_{exp}}{[1 + 2A_2M_wc + 3A_3M_wc^2 + 4A_4M_wc^3]_{master}} \quad (8)$$

This expression decreases indeed when $A_2 \rightarrow 0$. Still the left-hand side will not approach zero, when θ-conditions are reached. Even at $A_2 = 0$ the third virial coefficient remains positive. Thus, the effect of excluded volume screening seems to operate also for the branched macromolecules, but see below. We then turned to an examination of the concentration dependencies of the radius of gyration and the hydrodynamic radius.

Concentration Dependence of Radii. In a good solvent the measured apparent radii of gyration $R_{g,app}$ and hydrodynamic radii $R_{h,app}$ are influenced by repulsive interactions among the particles. The mathematical relationship between the apparent and the true radius of gyration at finite concentration is found as follows. The forward scattering is given as[20,21]

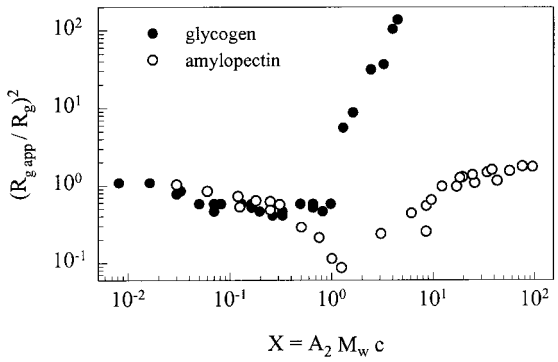

Figure 9. Concentration dependence of the apparent mean-square radius of gyration $R^2_{app}(c)$, normalized with respect of the radius of gyration R_g at infinite dilution. Symbols as in Figure 8.

$$\frac{Kc}{R_\theta} = \frac{1}{M_w}(1 + {}^1/_3R_g{}^2q^2) + 2A_2c + 3A_3c^2 \quad (9)$$

which can be transformed into

$$\frac{Kc}{R_\theta} = \frac{1}{M_w}[1 + {}^1/_3R_g{}^2q^2 + 2X + 3g_aX^2 + 4h_aX^3] \quad (9')$$

The apparent mean square radius of gyration is derived from the slopes in the Zimm plot as

$$R_g{}^2{}_{app}(c) = 3\,\frac{\text{slope}}{\text{ordinate}} \quad (10)$$

Applied to eq 8′, this leads to the following equation

$$R_g{}^2{}_{app}(c) = R_g{}^2(c)\frac{1}{M_w}\,\frac{M_w}{1 + 2X + 3g_aX^2 + 4h_aX^3} \quad (11)$$

and finally with eq 4′ to

$$R_g{}^2{}_{app}(c) = R_g{}^2(c)\frac{M_w}{M_{app}} \quad (12)$$

Figure 9 shows the result of the apparent radius of gyration $R_{g,app}$ and the corresponding true radius of gyration of the particles $R_g(c)$ at concentration c. As expected, the apparent radius decreased first with the concentration, but after correction for the repulsive interaction no significant change in the dimension was found (see Figure 10). At the overlap concentration c^* a very pronounced increase of the dimension is observed. Similar results were observed previously with amylopectin.[4] Notably the change in dimensions occurs in both cases almost exactly at c^*. However, the increase is less developed in the case of amylopectin than for glycogen. This appears to be an effect of the higher branching density in glycogen, in which the overlap of segment clouds from different molecules is more strongly restricted than in amylopectin with its lower branching density.

Also, the hydrodynamic radii $R_{h,app}$ change with concentration as a consequence of repulsive interaction. According to irreversible thermodynamics,[22−24] the concentration dependence of the mutual diffusion coefficient

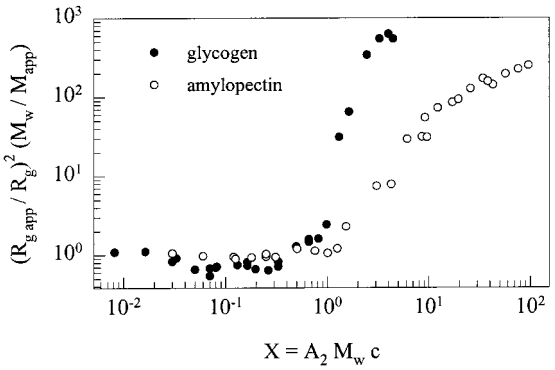

Figure 10. The same plot as in Figure 9, now corrected for the repulsive interaction. For further information see eq 11.

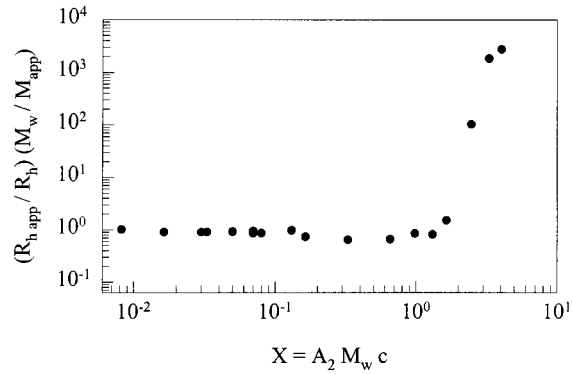

Figure 11. Concentration dependence of the hydrodynamic radius $R_{h,app}(c)$, normalized with respect of the hydrodynamic radius R_h at infinite dilution. The data are corrected for the repulsive interaction.

D_c is given as

$$D_c = \frac{kT}{6\pi\eta_0 R_h(c)}\left(\frac{M_w}{RT}\frac{\partial\pi}{\partial c}\right) \equiv \frac{kT}{6\pi\eta_0 R_{h,\,app}(c)} \qquad (13)$$

and from this equation it follows with eq 4′

$$R_h(c) = R_{h,app}\frac{M_w}{M_{app}} \qquad (14)$$

Note: the apparent hydrodynamic radius used in this paper is identical with the hydrodynamic correlation length ξ_h used by de Gennes.[1]

Figure 11 shows the result for the apparent $R_{h,app}(c)$ and the corrected $R_h(c)$ as a function of $X = c/c^*$. Again a sharp increase of the radius is observed, but now at a slightly higher concentration of about $2c^*$. The retarded onset may result from the fact that the hydrodynamic overlap concentration often does not completely agree with the static one.

In dilute solution the ratio $R_g/R_h \equiv \rho$ is a measure of the segment density in a macromolecule.[25] The value decreases with branching from $\rho = 1.7-2.0$ for linear chains to approximately $\rho \cong 1$ for hyperbranched samples. It appeared of interest whether the increase of the dimensions may be related to a change in the segment density. The plot in Figure 12 for the measured ρ parameter (after correction for *thermodynamic* interactions) remains constant up to c^*, passes then through a maximum, and decreases sharply beyond $X = 2$. The maximum can be explained by the difference in the static and dynamic overlap concentration. The steep decrease has probably two reasons of which one is

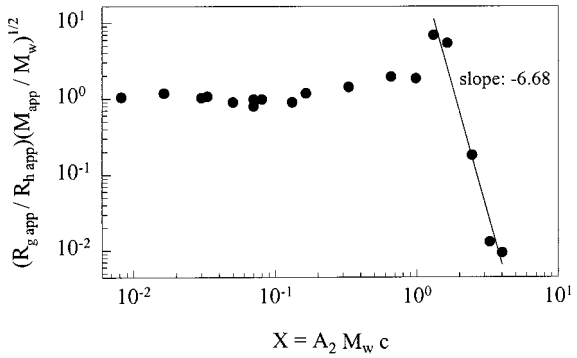

Figure 12. Concentration dependence of the ρ parameter $R_g(c)/R_h(c) \equiv \rho(c)$ for glycogen. The effect of repulsive thermodynamic interaction was split off, as is indicated by the notation of the ordinate. However, the hydrodynamic interaction remains still effective and finally becomes dominating.

dominating. First the segment density becomes very large beyond c^*, and second the frictional coefficient $f(c)$ has a concentration dependence, which in a first approximation is often written as

$$f(c) = f_{(0)}(1 + k_f c) \qquad (15)$$

with $f_{(0)} = 6\pi\eta_0 R_h$. The effect of the friction coefficient is certainly dominating, and the linear approximation of eq 15 will be no more sufficient. The smallest values obtained so far for the ρ parameter at dilute solution were obtained with microgels where $\rho = 0.3-0.5$.[26] In the present case, however, the decrease amounts to about a factor of 100. In fact, in the present case we are already in the highly "overlap" region, and here the friction is determined by disengagement of partially interpenetrated short chains from the particles. The increase of the friction coefficient in the overlap region now no longer follows a linear relationship but may tentatively be expressed by a power law

$$\frac{f(c)}{f(0)} \propto (c/c^*)^{6.7} \quad c > c^* \qquad (16)$$

The exponent 6.7 is an empirical value, and at present we cannot assign a special physical law to this value.

Concentration Dependence of the Molar Mass $M_w(c)$. The next point of interest was the actual molar mass $M_w(c)$ at a given concentration. As already outlined, around the overlap concentration deviations from the dashed line in Figure 2 were observed. The dashed curve represents the repulsive interaction of *nonassociated* glycogen molecules and amylopectin, respectively. The deviations to smaller values of M_w/M_{app} were tentatively explained by a screening of repulsive interactions. However, the drastic increase of the dimensions is certainly a clear indication of association. Large clusters combined with a slow motion in dynamic light scattering can, of course, be caused by metastable aggregates. In the present case, however, the clusters dissociate again on dilution, and therefore the cluster formation has to be considered as reversible and in thermodynamical equilibrium. The increase in radius must be connected with an increase in molar mass. An estimation for $M_w(c)$ of these associates can be made when fractal behavior is assumed for the particles. For nonaggregated amylopectins a fractal dimension of about $d_f = 2.3$ was found;[27,28] for the glycogens we found from SEC a value of $d_f = 2.8$.[8] With this fractal

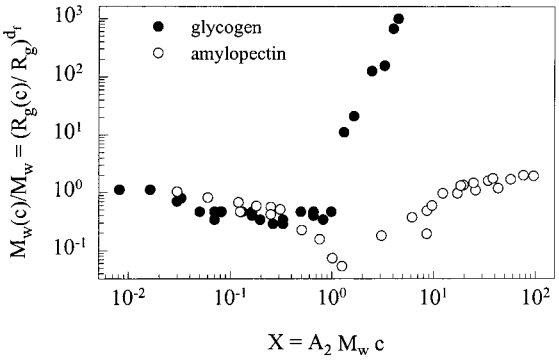

Figure 13. Increase of the molar mass $M_w(c)/M_w$ as a function of X for glycogen and amylopectin assuming fractal behavior for the associated clusters. $d_f = 2.8$ for glycogen and $d_f = 2.4$ for amylopectin.

assumption one obtains for the molar mass of the aggregates a relationship

$$\frac{M_w(c)}{M_w} = \left(\frac{R_g(c)}{R_g}\right)^{d_f} \tag{17}$$

Figure 13 shows the result as a function of X. Again, the increase in $M_w(c)$ is observed almost exactly at c^*. It is much more pronounced for glycogen than observed with amylopection. At this point it is essential to stress that in a mixture of particles mainly the large radii are measured by light scattering. Thus, the molar mass, calculated by eq 17, corresponds only to the aggregates. The overall weight average would be much smaller. Probably only a small fraction of associated particles are in equilibrium with nonassociated molecules.

Viscosity. The specific viscosity shows the expected concentration dependence. A slope around 1 was obtained for dilute solutions ($c < c^*$) and a very steep increase at $c > c^*$ with a slope around 5 (Figure 7). The intersection point of the two lines can be interpreted as the onset of hydrodynamic interactions, due to the hairy region in the outer shells of the particles. This intersection point occurs, however, at much lower values of $c[\eta]$ than known from linear chain molecules. For glycogen in 0.5 N NaOH and water we found $c[\eta] = 0.57$ and $c[\eta] = 0.82$, respectively. For linear nonassociated chain molecules, values of $c[\eta] = 4$ were found.[19] Evidently glycogen displays different behavior. Here it has to be mentioned that in contrast to other polymers the intrinsic viscosity of glycogen is very low ($[\eta] = 6.9$ mL/g) and shows no molar mass dependence. Both facts are typical for hard-sphere behavior. There was only a very weak shear rate dependency. For a concentration of 20% (mass/volume) the dynamic viscosity decreased from 0.0165 Pa s (at shear rate of 10 s^{-1}) to a value of 0.0155 Pa s (at shear rate of 650 s^{-1}). In principle, the value of $[\eta]$ can be described by a prolate elipsoide. However, the molar mass dependence of $[\eta]$ as reported in part 1[8] gave an exponent around ± 0, which is not consistent with the elipsoide but confirms hard-sphere behavior. Therefore, we compared our results with measurements in concentrated aqueous solution of latex particles.

Essentially the same behavior is observed up to c^* for glycogen in NaOH and water and for the latex particles.[29] Then a concentration follows, in which the viscosity of the latex suspension still coincides with the data of glycogen in water. At high concentrations the data from the latex particles start to diverge as expected, whereas the two curves for glycogen in water and 0.5 N NaOH are better described by power law behavior, which may be only an apparent one. This leads to the conclusion that the glycogens exhibit approximately hard-sphere properties. Probably a number of short dangling chains on the surface cause the difference in behavior at large concentrations. These will allow a certain segment interpenetration. Another interpretation would be that the freely swollen glycogen molecules become compressed at $c \gg c^*$ because of the very restricted interpenetration. At this point we wish to emphasize that the 15% (mass/volume) glycogen solution is certainly not similar to a melt. It is our opinion that the tube model, which is common for linear chains, is not found in the solution. All the ideas on reptation that we have for linear chains are in our view not applicable.

There should be a transition from the highly branched materials with nearly hard-sphere behavior to weakly branched materials and linear chains. So far known to us, the influence of branching density has not yet been studied systematically. We will look for other hyperbranched materials and will study the effects when the branching density is systematically varied. The presence of a small mass fraction of large associated particles has probably only a weak influence on η_{sp}, because both fractions seem to show hard-sphere behavior with no molar mass dependence of the intrinsic viscosity.

At the end we have to mention that almost nothing is known about the influence of polydispersity on the measured quantities in semidilute and concentrated regions. The effect may be important in the present sample, since the glycogen has a fairly broad size distribution, with a polydispersity ratio of $M_w/M_n \cong 30$.

Acknowledgment. We are grateful to the Deutsche Forschungsgemeinschaft for financial support of this work on the basis of an agreement with the Romania Academy. C.E.I thanks Professor Simionescu for suggesting her as an applicant. W.B. benefited much from a discussion with Dr. Jack Douglas on aggregation phenomena near and beyond the overlap concentration.

References and Notes

(1) De Gennes, P.-G. *Scaling Concepts in Polymer Physics*; Cornell University Press: Ithaca, NY, 1979.
(2) Daoud, M.; Martin, J. E. Mechanics of Formation of Fractal Objects. In *The Fractal Approach to Heterogeneous Chemistry*; Avenir, D., Ed.; Wiley: New York, 1992.
(3) (a) Trappe, V. Ph.D. Thesis, University of Freiburg, Germany, 1994; see also ref 5. (b) Trappe, V.; Burchard, W. *Polym. Prepr., Am. Chem. Soc., Div. Polym. Chem.* **1994**, *36*, 1.
(4) (a) Aberle, T.; Burchard, W. *Starch/Staerke* **1997**, *49*, 215. (b) Aberle, T.; Burchard, W. *Comput. Theor. Polym. Sci.* **1997**, *7*, 215.
(5) Burchard, W. *Adv. Polym. Sci.* **1999**, *143*, 113.
(6) Flory, P. J. *Principles of Polymer Chemistry*; Cornell University Press: Ithaca, NY, 1953.
(7) Freed, K. F. *Renormalization Group Theory of Macromolecules*; Wiley & Sons: New York, 1987.
(8) Ioan, C. E.; Aberle, T.; Burchard, W. *Macromolecules* **1999**, *32*, 7444.
(9) Galinsky, G.; Burchard, W. *Macromolecules* **1996**, *29*, 1498.
(10) Berne, B. J.; Pecora, R. *Dynamic Light Scattering*; Wiley & Sons: New York, 1976.
(11) McQuarrie, D. A. *Statistical Mechanics*; Harper & Row: Evanston, 1976.
(12) Friedman, H. L. *A Course in Statistical Mechanics*; Prentice-Hall: Englewood Cliffs, NJ, 1985.
(13) Burchard, W. *Makromol. Chem., Macromol. Symp.* **1988**, *18*, 1; **1990**, *39*, 179.
(14) Kosmas, M. K. *Macromolecules* **1989**, *22*, 720. See also the discussion in ref 9, p 1499, second paragraph on the right.

(15) Carnahan, N. F.; Starling, K. E. *J. Chem. Phys.* **1969**, *51*, 635.
(16) Ohta, T.; Oono, Y. *Phys. Lett.* **1983**, *79*, 339.
(17) (a) Trappe, V.; Burchard, W. Local Dynamics in Branched Polymers. In *Light Scattering and Photon Correlation Spectroscopy*; Pike, E. R., Abbis, J. B., Eds.; Kluwer Academic Publishers: Dordrecht, 1997; p 141. (b) Trappe, V.; Bauer, J.; Weismüller, M.; Burchard, W. *Macromolecules* **1997**, *30*, 2365.
(18) (a) Williams, G.; Watts, D. C. In *NMR, Principles and Progress*; Diehl, P., Fluck, E., Kosfeld, R., Eds.; Springer-Verlag: Berlin 1971; Vol. 4, p 271. (b) Kohlrausch, R. *Ann. Phys.* **1847**, *12*, 393. (c) Lindsey, C. P.; Patterson, G. D. *J. Chem. Phys.* **1980**, *73*, 3348.
(19) (a) Ross-Murphy, S. B. *Physical Techniques for the Study of Food Biopolymers*; Ross-Murphy, S. B., Ed.; Blackie Academic & Professional: Glasgow, 1994; Chapter 7. (b) Kulicke, W. M. Polymerlösungen. *In Fließverhalten von Stoffen und Stoffgemischen*; Kulicke, W. M., Ed.; Hüthig & Wepf: Basel, 1986; p 187.
(20) Equations 9 and 10 are essentially identical with a result derived by Benoit and Benmouna.[21] Their treatment again is equivalent to the random phase approximation.[1] All three approaches become identical when the excluded volume parameter v is identified as $v = (2A_2 + 3A_3c + 4A_4c^2 + ...)M_w$, and the correlation length ξ is given by $\xi = (1/3)^{1/2}R_g(c)$.
(21) Benoit, H.; Benmouna, M. *Polymer* **1984**, *25*, 1059.
(22) De Groot, S. R. *Thermodynamics of Irreversible Processes*; BI Hochschultaschenbücher: Mannheim, 1960; Vol. 18/18a.
(23) Yamakawa, H. *Modern Theory of Polymer Solutions*; Harper & Row: New York, 1971.
(24) Geissler, E. *Dynamic Light Scattering*; Brown, W., Ed.; Clarendon Press: Oxford, 1993; Chapter 11.
(25) Burchard, W.; Schmidt, M.; Stockmayer, W. H. *Macromolecules* **1980**, *13*, 1265.
(26) Schmidt, M.; Nerger, D.; Burchard, W. *Polymer* **1979**, *20*, 582.
(27) Hanselmann, R.; Burchard, W.; Ehrat, M.; Widmer, H. M. *Macromolecules* **1996**, *29*, 3277.
(28) Galinsky, G.; Burchard, W. *Macromolecules* **1995**, *28*, 2363.
(29) Senff, H.; Richtering, W. *J. Chem. Phys.*, in press.

MA991112H